NASA/TM–2013- 217513

Revision of the Atmospheric Delay Correction for ICESat-2 Laser Altimeter Ranges

L. Petrov and S. Luthcke

National Aeronautics and
Space Administration

Goddard Space Flight Center
Greenbelt, Maryland 20771

October 2013

NASA STI Program ... in Profile

Since its founding, NASA has been dedicated to the advancement of aeronautics and space science. The NASA scientific and technical information (STI) program plays a key part in helping NASA maintain this important role.

The NASA STI program operates under the auspices of the Agency Chief Information Officer. It collects, organizes, provides for archiving, and disseminates NASA's STI. The NASA STI program provides access to the NASA Aeronautics and Space Database and its public interface, the NASA Technical Report Server, thus providing one of the largest collections of aeronautical and space science STI in the world. Results are published in both non-NASA channels and by NASA in the NASA STI Report Series, which includes the following report types:

- TECHNICAL PUBLICATION. Reports of completed research or a major significant phase of research that present the results of NASA Programs and include extensive data or theoretical analysis. Includes compilations of significant scientific and technical data and information deemed to be of continuing reference value. NASA counterpart of peer-reviewed formal professional papers but has less stringent limitations on manuscript length and extent of graphic presentations.
- TECHNICAL MEMORANDUM. Scientific and technical findings that are preliminary or of specialized interest, e.g., quick release reports, working papers, and bibliographies that contain minimal annotation. Does not contain extensive analysis.
- CONTRACTOR REPORT. Scientific and technical findings by NASA-sponsored contractors and grantees.
- CONFERENCE PUBLICATION. Collected papers from scientific and technical conferences, symposia, seminars, or other meetings sponsored or co-sponsored by NASA.
- SPECIAL PUBLICATION. Scientific, technical, or historical information from NASA programs, projects, and missions, often concerned with subjects having substantial public interest.
- TECHNICAL TRANSLATION. English-language translations of foreign scientific and technical material pertinent to NASA's mission.

Specialized services also include organizing and publishing research results, distributing specialized research announcements and feeds, providing help desk and personal search support, and enabling data exchange services. For more information about the NASA STI program, see the following:

- Access the NASA STI program home page at http://www.sti.nasa.gov
- E-mail your question via the Internet to help@sti.nasa.gov
- Fax your question to the NASA STI Help Desk at 443-757-5803
- Phone the NASA STI Help Desk at 443-757-5802

NASA/TM–2013- 217513

Revision of the Atmospheric Delay Correction for ICESat-2 Laser Altimeter Ranges

Leonid Petrov
ADNET Systems, Inc., Greenbelt, MD

Scott Luthcke
NASA's Goddard Space Flight Center, Greenbelt, MD

National Aeronautics and
Space Administration

Goddard Space Flight Center
Greenbelt, Maryland 20771

October 2013

Level of Review: This material has been technically reviewed by technical management

Abstract

In 2001 *Herring and Quinn* proposed the algorithm for correction for atmospheric delay to ICESat-1 GLAS laser altimeter. The purpose of this document is to provide a revision of the algorithm suitable for processing the data from ICESat-2 mission scheduled for launch in 2016. The goal of the revision is to provide a procedure for atmospheric delay correction that would be precise to 1 mm level. The actual accuracy of delay computation will be somewhat less, but it will be limited only by imperfection of the used numerical weather model.

1 Introduction

In 2001 *Herring and Quinn* (2001) proposed the algorithm for correction for atmospheric delay to ICESat-1 GLAS laser altimeter. The purpose of this document is to provide a revision of the algorithm suitable for processing the data from ICESat-2 mission scheduled for launch in 2016. The goal of the revision is to provide a procedure for atmospheric delay correction that would be precise to 1 mm level. The actual accuracy of delay computation will be somewhat less, but it will be limited only by imperfection of the used numerical weather model.

2 Proposed changes

We propose to compute atmospheric path delay by integrating equations of wave propagation through the heterogeneous medium. Similar to the approach suggested by *Herring and Quinn* (2001), we will use numerical weather models for computing the refractivity field. We develop this approach further and suggest the following changes:

- Using numerical weather model GEOS-5.9.1 (FP-IT) instead of NCEP FNL model. The new model has a) better spatial and time resolution ($0.625^\circ \times 0.5^\circ \times 72 \times 3^h$ versus $1.0^\circ \times 1.0^\circ \times 27 \times 6^h$; b) semi-frozen status, i.e. lack of jumps due to model revision; c) better accuracy since it uses a more sophisticated theory that accumulates progress in our knowledge of atmosphere circulation acquired during last decade. Since GEOS (FP-IT) is provided at a terrain-following grid, the computational procedure to evaluate refractivity as a function of height is different.

- Computation of refractivity using rigorous algorithm of Ciddor (1996). *Herring and Quinn* (2001) claimed "the [Ciddor] algorithm requires a number of steps and as such as unsuitable for practical integration through the atmosphere". We do not agree with that statement and found that its implementation is neither difficult, nor computationally intensive.

- *Herring and Quinn* (2001) suggested to split path delay into two components, dry and wet, and integrate the first component analytically using a sort of ap-

proximation and to integrate the second component numerically. We compute the total path delay by rigorous integration the column of air refractivity.

- *Herring and Quinn* (2001) uses liner interpolation for computing refractivity at above the footprint. We expand the refractivity field into the four-dimensional B-spline basis. This ensures the continuity of path delay between nodes of interpolation.

2.1 Expression for refractivity of moist air

According to the definition, the refractivity is the ratio of the speed of propagation of electromagnetic wave in the media to the speed in vacuum. Therefore, integrating the refractivity along the path, we immediately get the path delay. The refractivity depends on the state of the atmosphere. For computation of refractivity with accuracy we need, $5 \cdot 10^{-4}$, we can consider all atmospheric gases, except water vapor, maintaining a fixed mixing ratio. The atmosphere can can be considered consisting of two components: dry and wet. Thereafter we select the following parameters that describes the state of the atmosphere: P — the total atmospheric pressure, P_w — the partial pressure of the water vapor, and T — air temperature, the so-called PPWTEM parameterization.

Detailed overview of the state-of-the-art of modeling refractivity is given in Rüeger (2002). The working group of the International Union of Geodesy and Geophysics on Fundamental Constants, issued a recommendation in 1991 that stated that "the group refractive index in air for electronic distance meter measurements to better than one part per million with visible and near infrared waves in the atmosphere be computed using the procedure published by Ciddor (1996) and Ciddor & Hill (1999).

The refractivity of moist air is computed according to Ciddor (1996)

$$n(P, P_w, T, k) = \frac{\rho_d(P, P_w, T)}{\rho_{d,r}} n_{d,r}(k) + \frac{\rho_w(P, P_w, T)}{\rho_{w,r}} n_{w,r}(k) \tag{1}$$

where $\rho_d(P, P_w, T)$ is density of dry component of the atmosphere as a function of total pressure P, partial pressure of water vapor P_w and air temperature, $\rho_w(P, P_w, T)$ is density of wet component, and $\rho_{d,r}$, $\rho_{w,r}$ are densities of dry air and water vapor at certain reference conditions. $n_{d,r}$ and $n_{w,r}$ are refractivity of dry air and water vapor at these standard conditions as a function of wave number which is reciprocal to wavelength $k = 1/\lambda$. Here, we define the refractivity as $\frac{c-v}{v}$, where c is the speed of light in vacuum and v is the speed of light in the medium.

Ciddor (1996) suggests the following equations for group refractivity $n_{d,r}$ and $n_{w,r}$ for reference meteorological conditions:

$$\begin{aligned} n_{d,r}(k) &= d_1 \frac{d_0 + k^2}{d_0 - k^2} + d_3 \frac{d_2 + k^2}{d_2 - k^2} \\ n_{w,r}(k) &= C \left(w_0 + 3w_1\, k^2 + 5w_2\, k^4 + 7w_3\, k^6\right) \end{aligned} \tag{2}$$

Reference meteorological conditions are $P = 101325$ Pa, $P_w = 0$, $T = 288.15$K for $n_{d,r}(k)$ and $P = 1333$ Pa, $P_w = 1333$ Pa, $T = 293.15$K for $n_{w,r}(k)$.

A general expression for the density of moist air endorsed by the International Committee for Weights and Measures (CIPM-2007) (Picard et al., 2007) is the following:

$$\rho_m = \left((P - P_w)\, M_d + P_w\, M_w \right) \frac{Z^{-1}(P, P_w, T)}{RT} \tag{3}$$

where M_d is molar mass of dry air, M_w is the molar mass of water, R is the universal gas constant and Z is air compressibility. The compressibility is computed this way:

$$\begin{aligned} Z(P, P_w, T) \;=\; & 1 \\ & - \frac{P}{T}\, (a_0 + a_1\, t + a_2\, t^2) \\ & + \frac{P_w}{T}\, (b_0 + b_1\, t) \\ & + \frac{P_w^2}{PT}\, (c_0 + c_1\, t) \\ & + \frac{P^2}{T^2}\, e_0 \\ & + \frac{P_w^2}{T^2}\, f_0 \end{aligned} \tag{4}$$

where $t = T + 273.15$. The coefficients are given in Table 1.

The expression for air refractivity can be regrouped to

$$n = \frac{S_d\, P \;+\; S_w\, P_w}{T}\, Z^{-1} \tag{5}$$

where

$$S_d = \frac{M_d}{R} \frac{n_{d,r}}{\rho_{d,r}}; \qquad S_w = \frac{M_w}{R} \frac{n_{w,r}}{\rho_{w,r}} - S_d \tag{6}$$

Thus, according to the rigorous algorithm for computing air refractivity in optical in near infrared range, path delay for ICESat-1 and ICESat-2 is computed using this expression:

$$n = \left(S_d(\lambda)\, \frac{P}{T} + S_w(\lambda) \frac{P_w}{T} \right) Z^{-1}(P, P_w, T) \tag{7}$$

where P is the total pressure, P_w is the partial pressure of water vapor, T is air temperature, S_d and S_w are parameters that depend only on wavelength and Z

Table 1. Used constants

d_0	$2.380185 \cdot 10^{+14}$	m^{-1}
d_1	$5.792105 \cdot 10^{+10}$	—
d_2	$5.7362 \cdot 10^{+13}$	m^{-2}
d_3	$1.67917 \cdot 10^{+09}$	—
w_0	$2.95235 \cdot 10^{-06}$	—
w_1	$2.6422 \cdot 10^{-20}$	m^{-2}
w_2	$-3.2380 \cdot 10^{-34}$	m^{-4}
w_3	$4.028 \cdot 10^{-47}$	m^{-6}
C	1.022	—
a_0	$1.58123 \cdot 10^{-6}$	$\mathrm{K} \cdot \mathrm{Pa}^{-1}$
a_1	$-2.933 \cdot 10^{-8}$	Pa^{-1}
a_2	$1.1043 \cdot 10^{-10}$	$\mathrm{K}^{-1} \cdot \mathrm{Pa}^{-1}$
b_0	$5.707 \cdot 10^{-6}$	$\mathrm{K} \cdot \mathrm{Pa}^{-1}$
b_1	$-2.051 \cdot 10^{-8}$	Pa^{-1}
c_0	$1.9898 \cdot 10^{-4}$	$\mathrm{K} \cdot \mathrm{Pa}^{-1}$
e_0	$1.83 \cdot 10^{-11}$	$\mathrm{K}^2 \cdot \mathrm{Pa}^{-2}$
f_0	$-7.65 \cdot 10^{-9}$	$\mathrm{K}^2 \cdot \mathrm{Pa}^{-2}$

Table 2. Coefficients of refractivity expression 5 for ICESat1 ($\lambda = 1064.0$ nm) and ICESat2 ($\lambda = 532.0$ nm):

	S_d	S_w
ICESat-1	$7.8147358 \cdot 10^{-7}$	$-1.0604128 \cdot 10^{-7}$
ICESat-2	$8.1822296 \cdot 10^{-7}$	$-9.7331360 \cdot 10^{-8}$

is the air compressibility. *Herring and Quinn* (2001) used a similar expression for refractivity:

$$n = S_d^a(\lambda)\,\frac{P}{T} + S_w^a(\lambda)\frac{P_w}{T} \tag{8}$$

but their parameters S_d^a, S_w^a slightly differ from Ciddor (1996) and they neglected compressibility Z. Direct tests showed that computation of refractivity using expression 7 takes 35 ns at a modern general purpose computer (I7-3930K @ 4.2GHz), which is a completely negligible share of the total computational budget.

2.2 Computation of refractivity field from NASA Global Modeling and Assimilation Office numerical weather models

At the moment, the NASA Global Modeling and Assimilation Office (GMAO) offers three models: MERRA Reanalysis, GEOS FP-IT, and GEOS-FP. The first model is

frozen. The output is updated monthly and has a lag of 20–50. GEOS FP-IT is semi-frozen and is updated 4 times a day with a lag of 9–15 hours. GEOS-FP is updated with the same schedule as GEOS FP-IT, but the model may undergo more frequency changes than GEOS FP-IT. All these models has a terrain-following vertical grid with 72 layers. The horizontal grid for MERRA is $0.5^\circ \times 0.667^\circ$, $0.5^\circ \times 0.5^\circ$ for GEOS (FP-IT) and $0.25^\circ \times 0.3125^\circ$ for GEOS-FP time resolution is 6 hours for MERRA and GEOS FP-IT, and 3 hours for GEOS-FP.

The output of GMAO numerical weather models at native grid does not provide parameters of the state of the atmosphere as a function of geometric height. Among other parameters, they provide specific humidity q, air temperature T, and so-called layer thickness at 72 layers. The layer thickness is defined as the difference in atmosphere pressure between layers. The atmospheric of the highest layer is fixed: 1 Pa. Therefore, the output of GMAO numerical weather models provide $T(P)$ and $q(P)$ as a function of pressure.

Assuming the atmosphere is in a state of the hydrostatic equilibrium and invoking the gas law, we write the differential state equation

$$\frac{dh}{dP} = \frac{R\,T(P)}{g(P)\Big(Z_d^{-1}(P,T)M_dP_d \;+\; Z_w^{-1}(P,T)M_wP_w\Big)} \tag{9}$$

where h is the geometric height, P is the atmospheric pressure which is decomposed into partial pressure of dry air P_d and water vapor pressure P_w, such that $P = P_d + P_w$, T is the air temperature, g is the gravity acceleration, Z_d^{-1} and Z_w^{-1} are compressibility of dry air and water vapor respectively, R is the universal gas constant, M_d and M_w are molar mass of dry air and water vapor.

Dependence of g on h is well known, for instance, (*Wahr*, 1996):

$$\begin{aligned} g(\varphi,h) = \;& g_e \frac{1+k\sin^2\varphi}{\sqrt{1-(2f_\oplus - f_\oplus^2)\sin^2\varphi}} \times \\ & \left[1 - \frac{2}{R_\oplus}\left(1 + \frac{\Omega_\oplus^2 R_\oplus^3(1-f_\oplus)}{GM} + (1-2f_\oplus)\sin^2\varphi\right)h + \frac{3}{R_\oplus^2}h^2\right]. \end{aligned} \tag{10}$$

Here $f_\oplus$ is the Earth's flattening, $R_\oplus$ is Earth's equatorial radius, φ — geodetic latitude, $\Omega_\oplus$ — Earth's angular velocity, GM — Earth's gravitational constants, and g_e, k are constants. But dependence g on P is determined by the solution of 9.

Equation 9 requires a boundary condition. The output of GMAO numerical weather model provides the so-called "surface geopotential" Φ. According to Bosilovich (private communication, 2011). $\Phi = h_o\, g^\star$, where h_o orthometric height of the 1st layer (surface), and $g^\star$ is the GMAO adopted gravity acceleration equal to 9.8 m/s^2. Therefore, the height above the ellipsoid of the 1st layer is $h_e = \frac{\Phi(\varphi,\lambda)}{g^\star} + \eta(\varphi,\lambda)$. Here $\eta(\varphi,\lambda)$ is the geoid undulation: the height of the geoid above the reference ellipsoid. We used EGM-2008 geoid undulations pre-computed at $1' \times 1'$ grid. We selected geoid undulations at the grid point nearest to the GMAO weather model grid point.

This differential equation is solved numerically with two iterations. Before the first iteration we tabulate $P(h)$ and $g(h)$ using the ISO Standard atmosphere (*ISO*,

1975) as a reference and found parameters of a linear regression between $\ln P$ and g. This gave us initial function $g(P) = -0.024942 + 0.002164 * \ln(P)$. Here pressure is in Pascal and gravity acceleration is in m/s^2. We used this expression for dependence of $g(P)$ in the first iteration. In our solution we set the air compressibility to 1, because the numerical weather models assume $Z = 1$, i.e. they treat the atmosphere as an ideal gas in its chain of data reduction and analysis. The hypsometric equation with $Z \neq 1$ will deviate from the model used for fitting atmospheric data and may cause undesirable biases.

For integration of 9 we use spline-interpolation of the function in the right-hand size and then express the integral through the coefficients of the spline. The solution gives us a table $h(P)$. Using this table, we compute an improved function $g(P)$ in its nodes and repeat integration. We stop iterations here, since the third iteration would result in changes in height at a level less than 0.1 meter. Inverting the table of solution, we get a table of the dependence of pressure on height above the reference ellipsoid.

As a result, we got P, T, and q as a function of ellipsoidal height, longitude, geodetic latitude, and time. Partial water vapor pressure P_w is computed from specific humidly and the total pressure $P_w = P \frac{q}{}(q + M_w/M_a)$, M_d and M_w are molar mass of dry air and water vapor. Using expression 7, we get the refractivity of moist air.

For further processing we need to represent refractivity as a continuous function of coordinate and time. We do it by expanding the refractivity field into a 4D basis. The only practical way to perform such an expansion is to recast the refractivity field into a suitable 4D *regular* grid. We define the area of the expansion as a shell between layers with fixed ellipsoidal heights: -1000 and 90,000 meters. We should notice that the height of native GMAP grid points increases with height exponentially. Therefore, using a uniform grid as a function of height will cause undersampling at the low altitude (and therefore, a loss of accuracy) and overampling at high altitude. To alleviate this problem, we perform a non-linear coordinate transformation and present n not as a function of height, but as a function of variable H defined as

$$H = \exp(h - \mu_3)/\mu_1 - \mu_2 \tag{11}$$

The coefficients: $\mu_1 = 20.25319, \mu_2 = 1200.0, \mu_3 = -169.30782$ produce a regular grid H in a range [-64, 64] that maps to heights [-1000, 90000] meters and approximately follows the vertical GMAO grid. We use 125 nodes, which is greater than 72 nodes of the original grid. Such oversampling guards us from losing precision during re-gridding.

To perform re-gridding, we compute the interpolating spline of $n(h)$ between the first and the last layer. For points of the new grid that follows in that range, we perform spline interpolation. For points below the first layer of higher than the last layer, we perform extrapolation. We assume temperature changes linearly with height at low atmosphere. In order mitigate the effects of boundary layers near the surface, we compute lapse rate $\frac{dT}{dh}$ using linear interpolation between the layers just 1000 m above the first layer and below 9000 m. Assuming the adiabatic law of

changing the state of the atmosphere with height, we extrapolate temperature and total pressure as

$$\begin{aligned} T(h) &= T(h_1) + \frac{dT}{dh}(h - h_1) \\ P(h) &= P(h_1) \left(\frac{T(h)}{T(h_1)} \right)^{-\frac{g(h) M_d}{R \frac{dT}{dh}}} \end{aligned} \tag{12}$$

For extrapolation of partial pressure of water vapour we make an assumption that relative humidity is not changing beneath the first layer, i.e.

$$\frac{P_w(h)}{P_s(P(h), T(h))} = \frac{P_w(h_1)}{P_s(P_1, T_1)}, \tag{13}$$

where $P_s(P, T)$ is the pressure the saturated water vapor. According to Picard et al. (2007), the vapor pressure at saturation is expressed via temperature and pressure as

$$P_s = (\alpha + \beta P + \gamma T) \, \exp(A\,T^2 + B\,T + C + D/T). \tag{14}$$

The coefficients in 14 are given in Table 3.

Table 3. Constants in equation 14.

α	1.0424	Pa
β	$3.14 \cdot 10^{-8}$	
γ	$5.6 \cdot 10^{-7}$	Pa K^{-2}
A	$1.2378847 \cdot 10^{-5}$	K^{-2}
B	$-1.9121316 \cdot 10^{-2}$	K^{-1}
C	$3.9371147 \cdot 10^{1}$	
D	$-6.3431645 \cdot 10^{3}$	K

We assume the atmosphere is isothermal near the upper level and therefore, pressure obeys the following law:

$$P(h) = P(h_t) \exp\left(-\frac{g(h) M_d}{R} (h - h_t) \right). \tag{15}$$

Equation 12 extends the numerical weather model to the area which it does not cover, but they mainly affect areas under the surface which do not have phisical meaning. However, there are two situations when extrapolated atmospheric parameters are actually used. Firstly, the Earth surface altitude used by the GMAO models and by ICESat are not exactly the same. There are areas where the ICESat surface is beneath the GMAO surface. Secondly, in mountainous regions some nodes

of the grid may fall in ridges. The surface height in valleys may appear beneath the height of surrounding grid nodes.

Finally, the coefficients of of the expansion of the refractivity index over the tensor products of B-splines are computed using the values of the refractivity at grid point:

$$n(h,\lambda,\varphi_{gd},t) = \sum_{i=1-m}^{i=d_1-1} \sum_{j=1-m}^{j=d_2-1} \sum_{k=1-m}^{k=d_3-1} \sum_{l=1-m}^{l=d_4-1} N_{ijkl}\, B_i^m(h)\, B_j^m(\lambda)\, B_k^m(\varphi_{gd})\, B_l^m(t), \quad (16)$$

where $B_s^m(x)$ is the basis spline function of variable x of degree m with the pivot node s, and d_1, d_2, d_3, d_4 are dimensions. The problem of evaluation of the 4D fields of the coefficients of expansion N_{ijkl} is reduced to solving systems of banded linear algebraic equations over 1st, 2nd, 3rd and 4th dimension with multiple right hand sides. There exists an extremely efficient algorithm for this computation.

2.3 Computation of path delay using the refractivity field

Computation of path delay in zenith direction is performed by numerical integration of the refractivity along the vertical direction from the surface height defined by ICESat measurement and the highest layer. Since variables h, λ, φ, and t are independent, integral over variable h

$$d = \sum_{j=1-m}^{j=d_2-1} \sum_{k=1-m}^{k=d_3-1} \sum_{l=1-m}^{l=d_4-1} B_j^m(\lambda)\, B_k^m(\varphi_{gd})\, B_l^m(t) \sum_{i=1-m}^{i=d_1-1} \int_{h_s}^{h_t} N_{ijkl}\, B_i^m(h)\, dh. \quad (17)$$

We introduce function

$$I_k^m(x) = \int_x^{+\infty} B_k^m(x), \quad (18)$$

which is computed similar to $B_k^m(x)$ through a recurrent relationship. Notice that $B_k^m(x)$ is non-zero only at $m+1$ knots in the vicinity of the grid point closest to the x, but not exceeding x, Then we can write integral 17 elegantly:

$$d(h,\lambda,\varphi_{gd},t) = \sum_{i=i_p-m}^{i=d_1-1} \sum_{j=j_p-m}^{j=j_p} \sum_{k=k_p-m}^{k=k_p} \sum_{l=l_p-m}^{l=l_p} N_{ijkl}\, I_i^m(h)\, B_j^m(\lambda)\, B_k^m(\varphi_{gd})\, B_l^m(t), \quad (19)$$

where i_p is maximum i that $h_i < h$, j_p is maximum j that $\lambda_j < \lambda$, k_p is maximum k that $\varphi_i < \varphi$, and l_p is maximum l that $t_l < t$.

During processing ICESat data, we do not know the surface height precisely. We see from the definition of path delay d that its derivative over height is just air

refractivity. It is computed as

$$\frac{\partial d(h,\lambda,\varphi_{gd},t)}{\partial h} = n = \sum_{i=i_p-m}^{i=i_p} \sum_{j=j_p-m}^{j=j_p} \sum_{k=k_p-m}^{k=k_p} \sum_{l=l_p-m}^{l=l_p} N_{ijkl}\, B_i^m(h)\, B_j^m(\lambda)\, B_k^m(\varphi_{gd})\, B_l^m(t). \quad (20)$$

That derivative is used when we need to correct path delay for update of the surface height with respect to its a priori value. If the height correction is too large, the contribution of the second derivative may appear substantial. In order to evaluate the contribution of the second derivative of delay with height, which is equal to the first derivative of refractivity with height, we compute it using the ISO standard atmosphere at the sea level: $\frac{\partial^2 d}{\partial h^2} = \text{-}2.7 \cdot 10^{-8}$ m^{-1}. The contribution will reach 1 mm, when the height correction exceeds 270 m.

ICESat shoots not in nadir, but at the angle z which does not exceed 5°. Assuming the atmosphere is flat, the path delay at zenith angle z depends on path delay in zenith direction as $d(z) = d_z/cos(z)$. *Herring and Quinn* (2001) showed the deviation of the dependence of path delay on zenith angle from sec z introduces errors less than 0.1 mm, which is negligible.

3 Comparison of path delay for ICESat-1 data computed with two methods

We compared computation of ICESat-1 path delay made according to the procedure of *Herring and Quinn* (2001) and made using the procedure described above. The origin of differences in path delay are a) differences in the algorithms and b) because differences in numerical weather models. In order to distinguish these two factors, we computed path delay using the new algorithms but the old numerical weather model: NCEP FNL. Then we computed the path delay using the same (new) algorithm, but different weather models.

3.1 Effect of differences in the computational procedure on path delays

We computed path delay for ICESat-1 ice dataset over Antarctica and Greenland using geolocation of the footprint and time from the ICESat-1 data files GLAH14. We used the output of numerical weather model NCEP FNL for this test — exactly the same files that were used previously.

Figures 1–4 show typical differences for dry and wet path delays. Wet path delay over Antarctic and Greenland is typically below 1 mm. Since the digitization errors of path delays stored in GLAH14 ICESat-1 data files is 1 mm, comparison does not reveal much useful information.

The differences in the contribution of dry air in path delay show 1) slow variations, 2) jitter with amplitude 15-20 mm that is always negative; 3) jumps due to digitization errors of 1 mm.

Figure 1. The **raw differences** between dry path delays embedded ICESat-1 data files and those computed from the FNL numerical weather model using new algorithm. The **blue curve** shows them smoothed with a Gaussian running fitter.

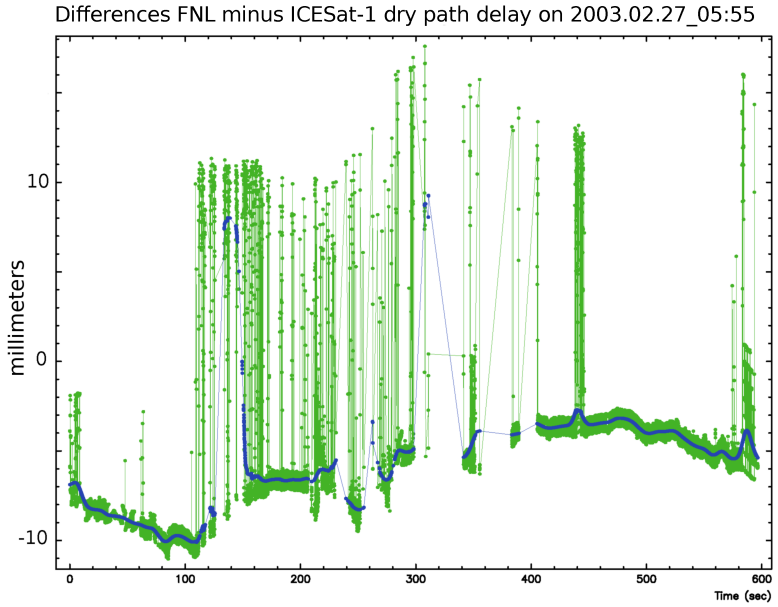

Slow variations are explained by differences in interpolation of the atmospheric field, by more refined expressions for air refractivity that accounts for air compressibility, and by integration technique.

Figure 2 clearly shows that the jitter is present only in path delay computed following the old procedure. We tried to extract the jitter by smoothing the path delay with a Gaussian filter and making the distribution of outliers exceeding 8 mm. Outliers less than 8 mm are difficult to extract with an automatic procedure since they are comparable with errors of smoothing. We present the plot of distribution of outliers in Figure 5. The peak of outliers is at 14 mm and the frequency of outliers drops to zero at 24 mm. Difference in path delay 14 mm may be caused by a differences in the altitude of the footprint at the amount of 50 m. At the moment, we do not have an explanation what causes a jitter. We suspect it might be caused by a bug in software.

Computation speed was measured using a typical ICESat-1 daily datafile GLAH12_633_2115_003_0365_0_02_0001.H5 that contains 325,000 good data points. At computer i7-3930K @ 4.2 GHz execution wall time was 180.1 s + 8.9 mks per point, in total 182.9 s using one core and 58.2 s + 1.5 mks per point, in total 58.2 s using all six cores.

Figure 2. Dry troposphere path delay, **embedded in ICESat-1 data** and **computed from FNL numerical weather** at day 2003_02_26_GLAH12_633_1102_002_0043_0_02_0001. We see a) bias between **blue** and **green** curves; b) digitization errors in **green curves**; and c) jitter in **green curve** between seconds 160 and 169. Time argument 0 in plots corresponds to 2003.02.27-18:02:30.0331370085 TAI.

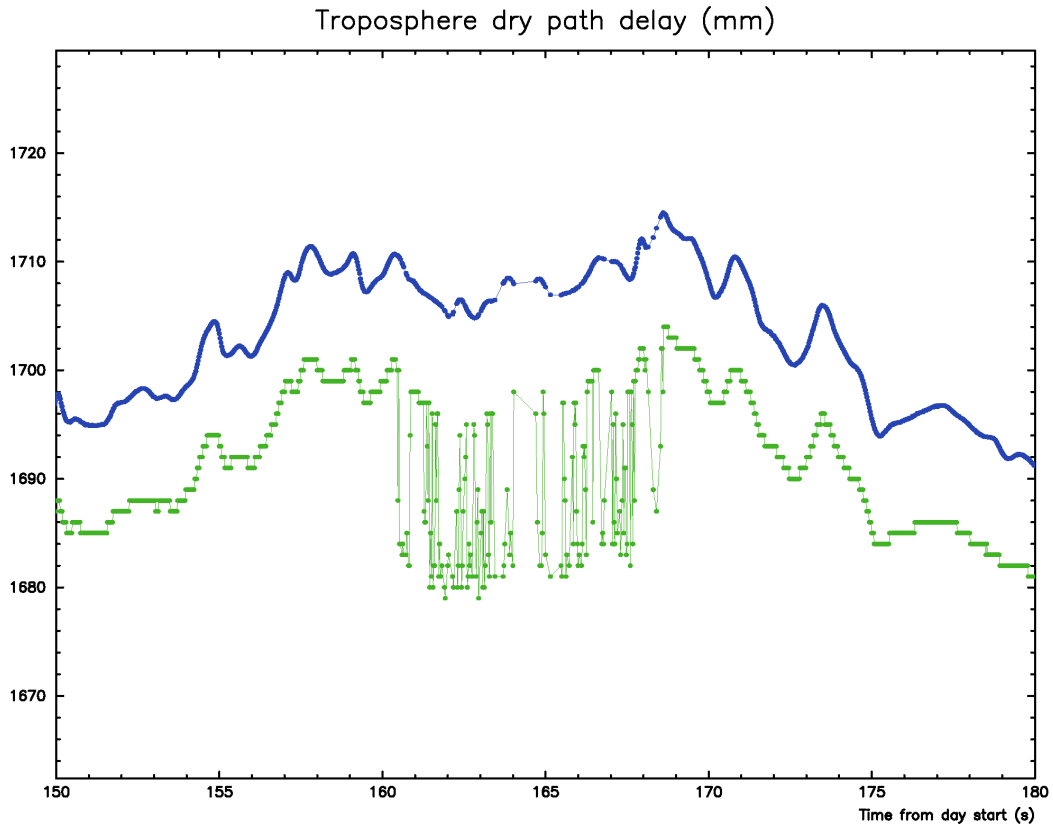

3.2 Time and area-averaged differences

In order to evaluate the effect of differences in the computational procedure on ice mass estimates, we computed path delay for every valid ICESat-1 shot. Then we averaged the differences in time over cells of the equi-area grid with cell size around 20 km. The results for Antarctica are shown in figure 6.

Then we averaged the differences over the area of Antarctica and Greenland. The differences were also averaged over one day (Figure 7, left side) and over each campaign (Figure 7, right side)

Figure 3. The **raw differences** between wet path delays embedded ICESat-1 data files and those computed from the FNL numerical weather model using new algorithm. The **blue curve** shows them smoothed with a Gaussian running fitter.

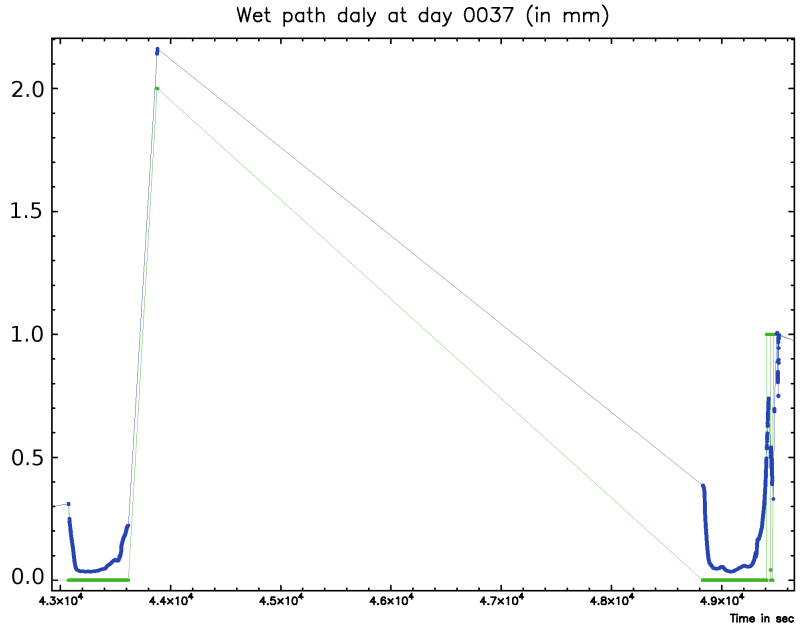

3.3 Contribution of differences in numerical weather models to path delay

We computed path delay using the new algorithm with two numerical weather models, NCEP FNL (as it was in original ICESat-1 data analysis) and MERRA. The mean differences, the rms and linear trend are shown in Figures 8 and 9. The differences in path delay averaged over Antarctica and over time of each ICESat-1 campaign are shown in Figure 10.

4 Concluding remarks

We have developed a new algorithm for computing path delay using numerical weather models with precision better than 1 mm and accuracy determined by the errors of numerical weather models. We found that the old computational procedure proposed by *Herring and Quinn* (2001) have a bias at a level of 10–40 mm with 1.3% points affected by a jitter with mean values -14 mm. The average bias of differences is 12–15 mm and rms 4–6 mm. The differences have a liner trend 1–2 mm/yr. Both biases, rms, and trend show a patter of spatial coherence. Approximately 1/3 of the bias and rms stems from the differences in the algorithm of computing the path delay and 2/3 is due to differences are numerical weather models.

The comparison shows that the jitter is present only in path delays computed with the old procedure. Therefore, we conclude tentatively that this is the error

in the old procedure, possibly caused by a bug in software. Aside the jitter, the comparison tests cannot prove which algorithm is more accurate. Indirect pieces of evidence, a) using rigorous formulae for refractivity of moist air, b) using a rigorous procedure for 4D interpolation of the gridded output of meteorological parameters; c) using numerical weather that are more sophisticated and have significantly higher resolution suggest the proposed approach has a better accuracy. The old computation procedure had errors of $\sim 1 - 4$ cm, the differences in the algorithm itself contributing at a level of 6–10 mm on average. The new procedure is essential to reducing the error budget caused by the atmosphere to a millimeter level.

5 References

International Organization for Standardization, Standard Atmosphere, ISO 2533:1975, 1975

P. Ciddor, Refractive index of air: new equations for visible and near infrared, Applied Optics, 35(9), 1566–1573, 1996

Ciddor, P.E. & Hill, R.J, Refractive Index of Air. 2. Group Index, Applied Optics, 38(9), 1663–1667, 1999

Herring, T.A., K. Quinn, Atmospheric Delay correction to GLAS laser altimeter ranges, ATBD, Version 2.1, 2001

Picard, A., R.S. Davis, M. Gläser, and K. Fujii, Revised formula for the density of moist air (CIPM-2007), Metrologia, 45, 149–155, 2007

Rüeger, J. M., Refractive indices of light, infrared and radio waves in the atmosphere, UNISURV S-68, report from School of Surveying and Spatial Information System, Uni. of New South Wales, Sydney, Australia, 2002

Wahr, J., Geodesy and Gravity: Course Notes, 1996, Samizdat Press

Figure 4. Differences between dry path delay embedded in ICESat-1 data at day 2003_02_26_GLAH12_633_1102_002_0043_0_02_0001 and those computed using the new algorithm and old NCEP FNL model. The upper plot shows 340,000 differences over one day. The low plot shows 2800 differences over 70 seconds. Time argument 0 in plots corresponds to 2003.02.27-18:02:30.0331370085 TAI.

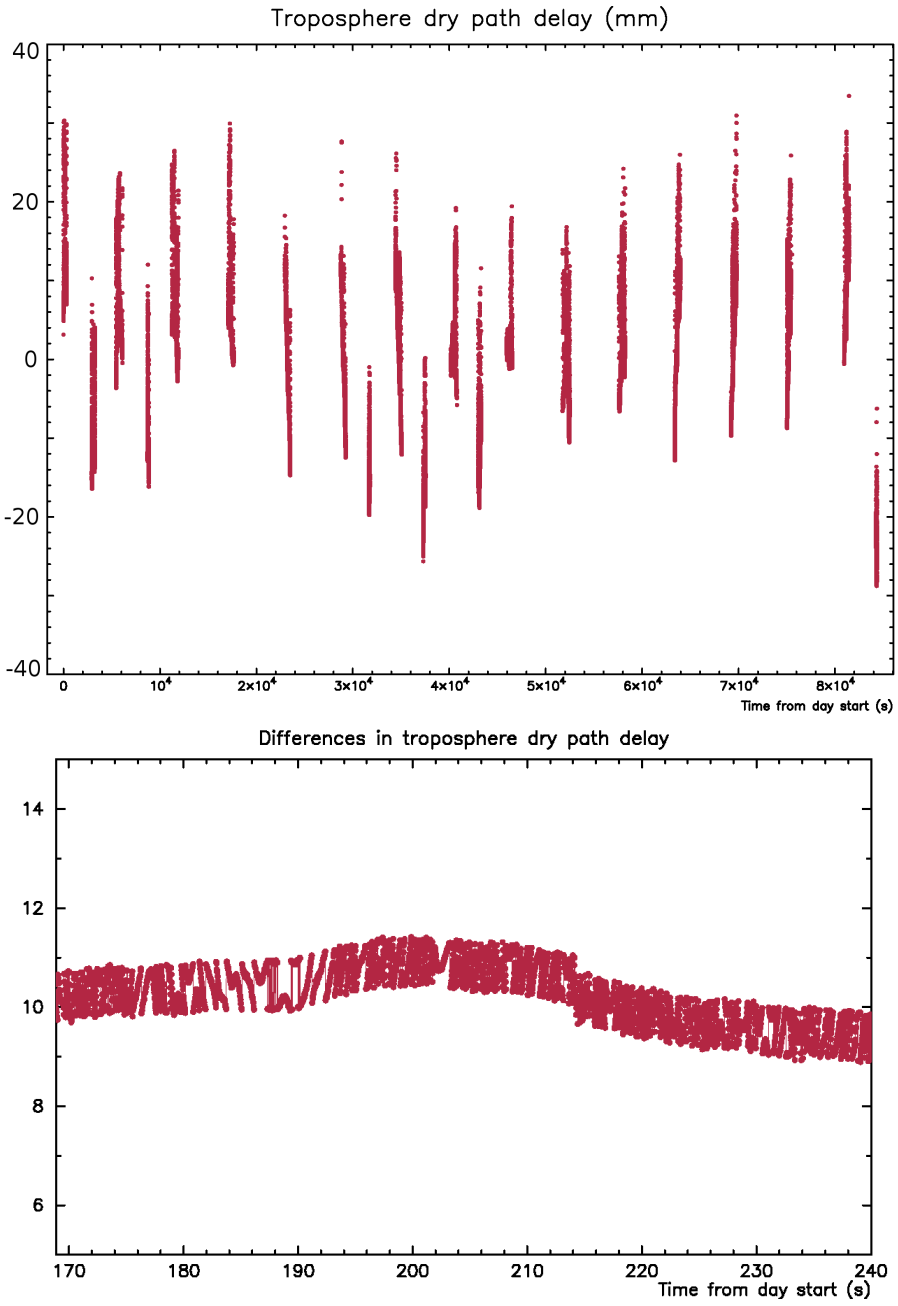

Figure 5. The dry delay embedded in ICESat-1 data were smoothed with a Gaussian running fitter. The distribution of the differences between smoothed values and row data is shown in the plots. The differences less than 8 mm were not taken into account since the filter does not separate normal points and small outliers reliably.

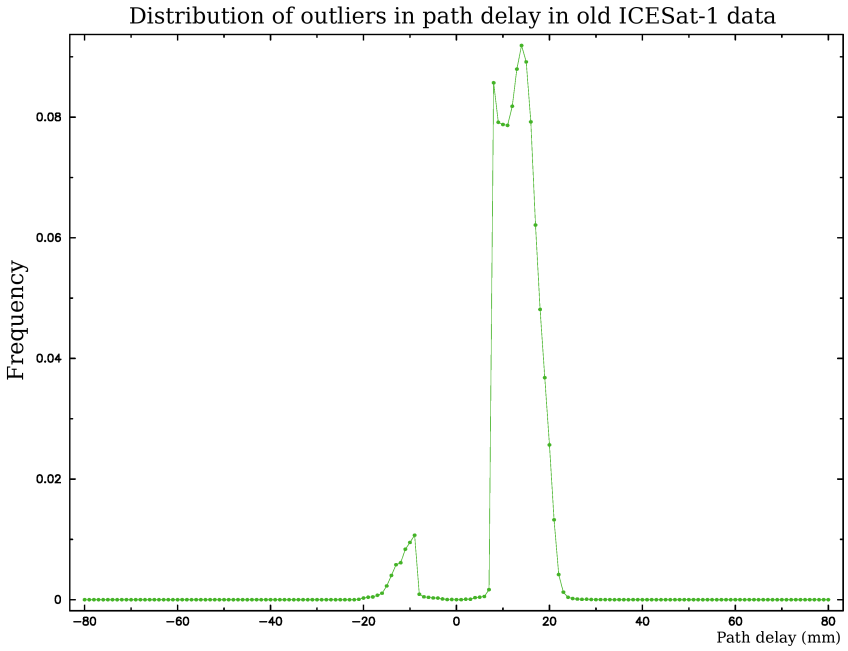

Figure 6. The mean and rms of differences of dry path delay embedded in ICESat-1 data and computed from FNL numerical weather model before and after outlier rejection. The points are averaged over all time epochs. The size of equi-area cells is around 20 km. The left plot shows the mean without outlier rejection, the right plot shows the mean after outlier rejection. The upper row shows the mean, the low row shows the rms.

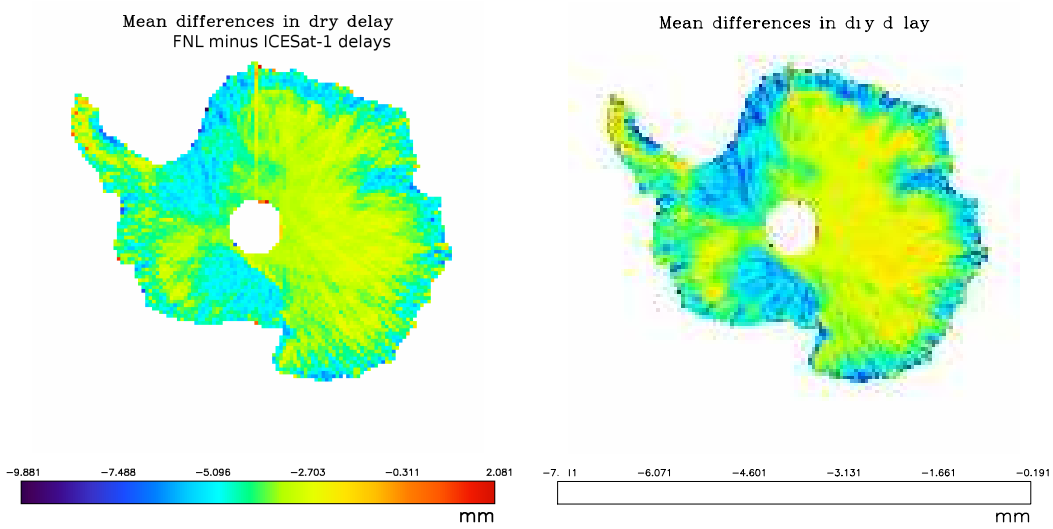

Figure 7. **Area averaged differences** in path delay computed with the new algorithm and using numerical weather models NCEP FNL and MERRA. *Upper row:* Mean differences of dry path delay over the ice for every day. *Low row:* Mean differences of dry path delay over the ice for every campaign. *Left column* shows differences for Antarctica. *Right column* shows differences for Greenland. NB: scales are different.

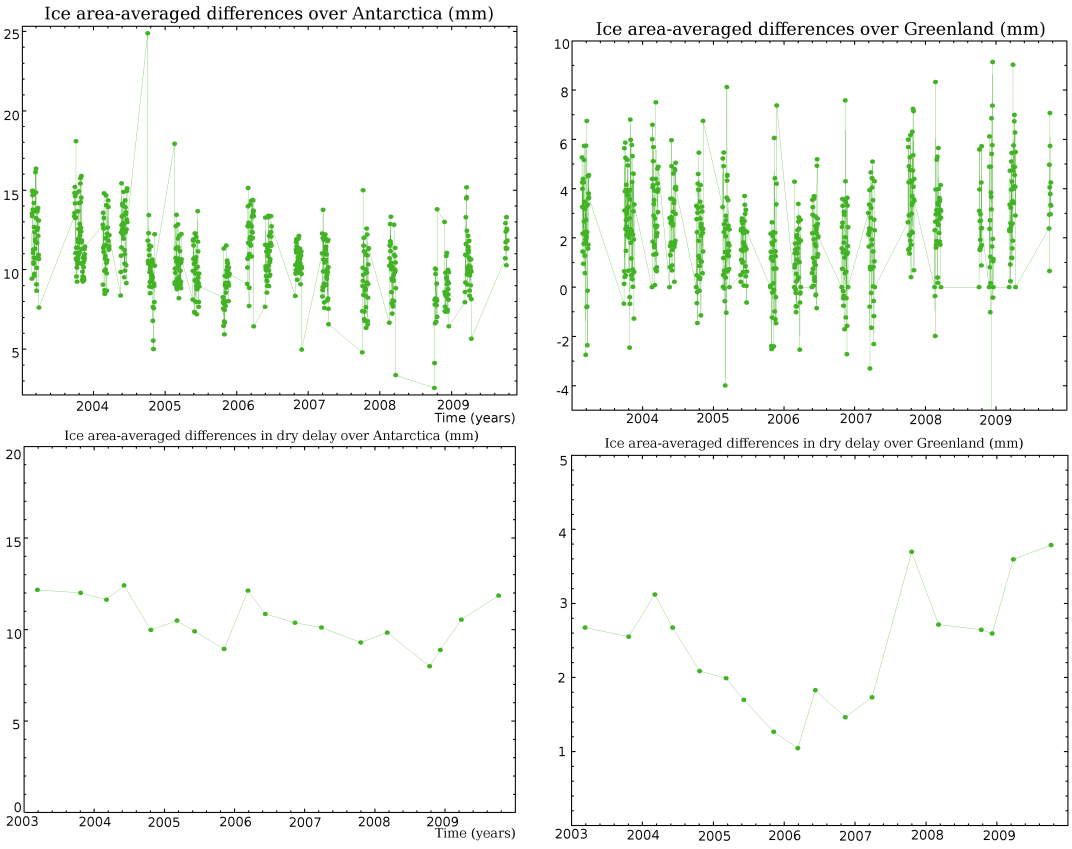

Figure 8. The mean differences of path delay computed using the new algorithm with MERRA and FNL numerical weather models at epochs of ICESat-1 shots, averaged over times.

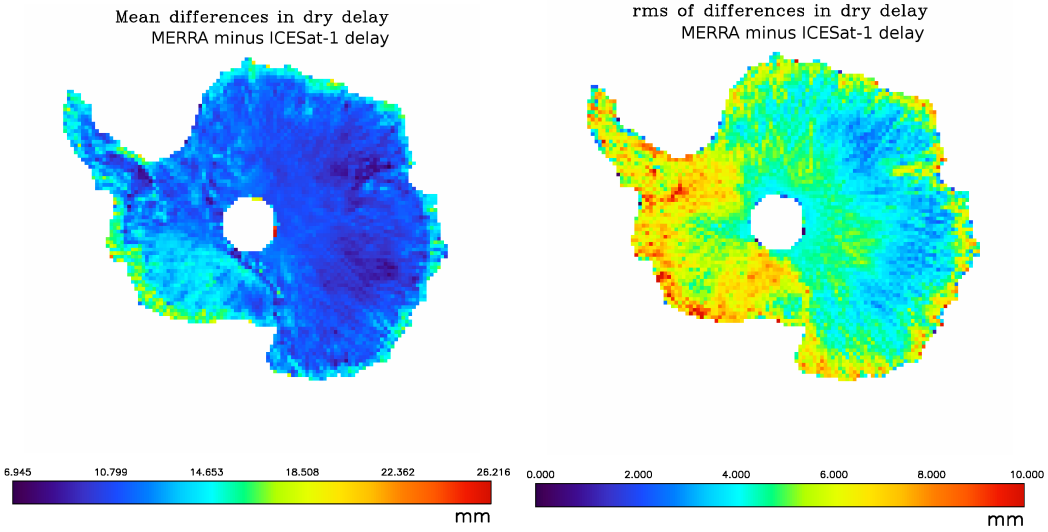

Figure 9. The linear trend in path delay computed using the new algorithm with MERRA and FNL numerical weather models over all epochs of ICESat-1 shots.

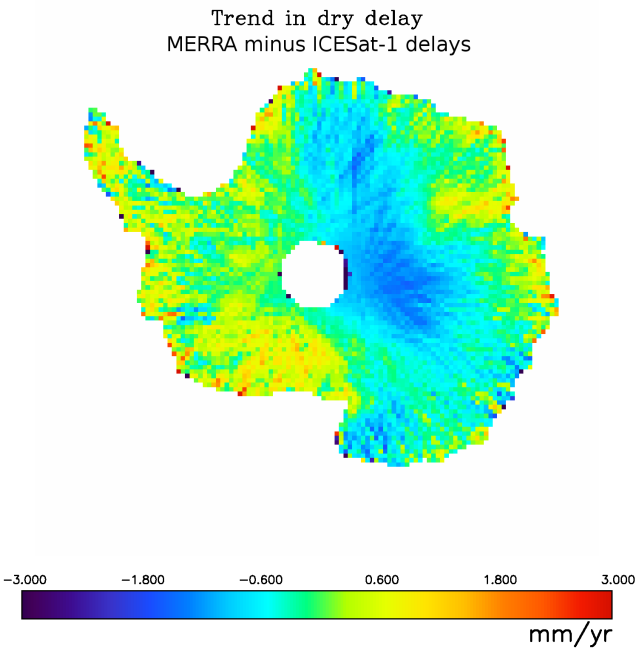

Figure 10. Differences in path delay averaged over Antarctica computed using the new algorithm with MERRA and FNL numerical weather averaged over time of individual campaigns.

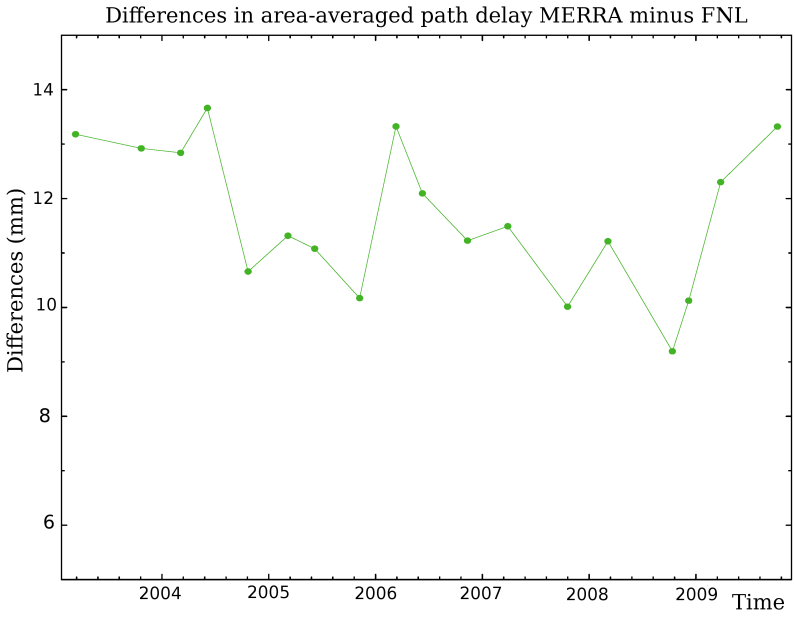

REPORT DOCUMENTATION PAGE

Form Approved
OMB No. 0704–0188

1. REPORT DATE *(DD-MM-YYYY)*	2. REPORT TYPE	3. DATES COVERED *(From - To)*
01-10-2013	Technical Memorandum	

4. TITLE AND SUBTITLE
Revision of the atmosperic delay correction for ICESat-2 laser altimeter ranges

5a. CONTRACT NUMBER

5b. GRANT NUMBER

5c. PROGRAM ELEMENT NUMBER

6. AUTHOR(S)
Leonid Petrov and Scott Luthcke

5d. PROJECT NUMBER

5e. TASK NUMBER

5f. WORK UNIT NUMBER

7. PERFORMING ORGANIZATION NAME(S) AND ADDRESS(ES)
NASA Goddard Space fight Center
Greenbelt, Marlyland 20771

8. PERFORMING ORGANIZATION REPORT NUMBER

9. SPONSORING/MONITORING AGENCY NAME(S) AND ADDRESS(ES)
National Aeronautics and Space Administration
Washington, DC 20546-0001

10. SPONSOR/MONITOR'S ACRONYM(S)
NASA

11. SPONSOR/MONITOR'S REPORT NUMBER(S)
NASA/TM–2013–217513

12. DISTRIBUTION/AVAILABILITY STATEMENT
Unclassified-Unlimited
Subject Category ?
Availability: NASA CASI (443) 757-5802

13. SUPPLEMENTARY NOTES
Last revised on 2013.10.24 23:58:50
An electronic version can be found at http://ntrs.nasa.gov.

14. ABSTRACT

In 2001 *Herring and Quinn* proposed the algorithm for correction for atmospheric delay to ICESat-1 GLAS laser altimeter. The purpose of this document is to provide a revision of the algorithm suitable for processing the data from ICESat-2 mission scheduled for launch in 2016. The goal of the revision is to provide a procedure for atmospheric delay correction that would be precise to 1 mm level. The actual accuracy of delay computation will be somewhat less, but it will be limited only by imperfection of the used numerical weather model.

15. SUBJECT TERMS
ICESat, atmosphere path delay

16. SECURITY CLASSIFICATION OF:			17. LIMITATION OF ABSTRACT	18. NUMBER OF PAGES	19a. NAME OF RESPONSIBLE PERSON
a. REPORT	b. ABSTRACT	c. THIS PAGE			Scott Luthcke
U	U	U	UU	26	19b. TELEPHONE NUMBER *(Include area code)* 301.614.6112